RSC Advances

Preparation and Rheological Properties of Whey Protein Emulsion Fluid Gels

Journal:	*RSC Advances*
Manuscript ID:	RA-ART-06-2015-012684
Article Type:	Paper
Date Submitted by the Author:	30-Jun-2015
Complete List of Authors:	Moakes, Richard; University of Birmingham, School of Chemical Engineering Sullo, Antonio; University of Birmingham, School of Chemical Engineering Norton, I; The University of Birmingham, School of Engineering

Preparation and Rheological Properties of Whey Protein Emulsion Fluid Gels

R. J. A. Moakes*, A. Sullo, I. T. Norton

Centre for Formulation Engineering, School of Chemical Engineering, University of Birmingham, Edgbaston, Birmingham, B15 2TT, UK

*Corresponding Author: rjm116@bham.ac.uk

Abstract

A shear-gel approach was used to coat an O/W emulsion with a whey protein shell. Mechanical shear was applied to an aqueous solution of whey protein isolate (WPI) and oil then heated through the sol-gel transition. The formation of a continuous WPI network was prevented through the shear flow, resulting in discreet spherical capsules, with sizes in the micron scale (~25 μm). Through careful control over both the oil and WPI components, encapsulation efficiencies of up to 99% were obtained. Subsequent rheological properties highlighted elastic behaviour (G') dependent on oil content; where higher oil fractions increased the effective phase volume of the particles. The result was packing fractions that exceeded those for hard spheres (>0.64), leading to pseudo-solid characteristics at rest, apparent yield stresses and thixotropic behaviour under shear. As such, emulsion fluid gel (EmFG) rheology was closely comparable to those of soft microgel suspensions (fluid gels) and soft-coated particles.

Keywords

Whey Protein Isolate/WPI; Emulsion; Fluid/Shear Gels; Encapsulation; Material Properties; Rheology

1. Introduction

The use of particulates as rheological modifiers spans across multiple industries: paint, cosmetic, food etc. For this reason, systems such as colloidal suspensions and emulsions have been well documented. However, more recently microparticulate gel suspensions have received increasing interest for their ability to create weakly structured fluids, with rheological properties characterised between those for colloidal particles and polymeric gels; pseudo-solid behaviour at rest, but flow above a critical stress[1-4]. Enhanced flow behaviours have been observed in polysaccharide fluid gels where, at volume fractions as low as ϕ 0.2 suspensions showed high viscosities and marked shear thinning behaviour, typical of highly aggregated systems[5, 6]. The observed changes in flow properties were assigned to the particle microstructures, where, as a result of incomplete gelation at the particle surface, interactions between microgel spheres resulted in a degree of structuring. Additionally, the deformability of such soft hydrogel particles led to volume fractions that exceeded those typical for hard spheres. At such high volume fractions particles become sterically confined, thus rheology became more closely governed by the particle moduli[7-9].

Particle intrinsic properties such as strength and deformability can be better understood by looking at a comparable quiescently formed gel. Again, mechanical properties are closely linked to the gel microstructure[10-14]. Complex microstructures therefore provide another means of controlling a gel's

physicomechanical properties. Besides polymer mixes where two or more polymers undergo a sol-gel transition, filler particles can be used to prepare gel composites[15]. These composites display viscoelastic properties as a function of the gel matrix, volume fraction and rigidity of the filler. Chemical affinity between the filler and surrounding substrate is also very important[16]. Typically, where the filler interface is included into the gelled network strengthening of the matrix occurs[17]. It was demonstrated that increasing the time scale between emulsification and gelation resulted in a shift from stronger to weaker gels. Here, polymerisation of the emulsifier lowered the affinity between oil filler and substrate matrix, causing inherent weak spots within the gel[17-19].

Processing is therefore a major consideration in the preparation of gels, on both a macro and micro-scale. Microgels are typically formed by confining the polymer during the sol-gel transition. This can be achieved by means of chemical[20] or mechanical[1] separation. Controlled microstructures and further rheological properties can be achieved by a microstructural design approach; whereby changing the formulation, *i.e.* composition, degree of cross-linking and system pH, leads to careful control over the gelled network[4, 21]. Additionally, in the case of shear gels, modulating the two processing parameters shear and thermal history can lead to controlled particle size and morphology. When the separation applied to the system is such that it becomes comparable to the timescale for polymer ordering, random coil to helix transition and subsequent gelation through the formation of junction sites, thermodynamically favourable spherical particles (~1 μm) are formed: where the enthalpies of melting are much smaller to comparable quiescently prepared gels[22]. The rate of particle growth therefore becomes key. Large anisotropic (~100 μm) particles form

when structuring is so rapid that initial gels are able to form, becoming subsequently broken down in the shear flow. However, in whey protein systems an inverse relationship between aggregation kinetics and system elasticity was observed, showing faster rates to yield weaker suspensions, with lower yield stresses and viscosities[23].

Supramolecular chemistry has also shown a viable route to the preparation of micro-composites[24-26]. These particles are formed through electrostatic bonding of the polymers. The particulates are formed by carefully controlling the pH so that the zeta-potential of both polymers is of an opposite charge, with a potential great enough to drive complexation. Such micro-particulates, based on an $O/W_1/W_2$ system, exhibited a several fold increase in viscosity when compared to a simple O/W emulsion[24]. These viscosity changes were attributed to a change in the effective phase volume of the hydrogel spheres, which were further increased through the inclusion of an oil filler. However, interactions between the particles were not observed.

We report here the preparation of emulsion fluid gel (EmFG) particles, a micro-composite of whey protein gel and oil. The research builds on work presenting $O/W_1/W_2$ filled hydrogel systems by applying a "shear gel approach" to promote interactions between resulting particles. As such, it takes an additional step to surfactant or Pickering stabilised emulsions by gelling a continuous WPI layer around an oil core. The technique applied results in an elastic suspension, whereby the particles become trapped, suspended in an aqueous phase. Unlike similar studies[27] the final systems act in a pseudo-solid fashion until a great enough stress is applied to induce flow, thinning the suspension into a liquid-like state. The microparticles thus offer the capacity to

act as a multifunctional composite, for both controlled rheological applications and pose the potential to encapsulate poorly soluble molecules.

The work focuses on whey protein isolate (WPI) as the coating material owing to its thermo-denaturation and subsequent hydrophobic aggregation, to form a gel layer on the surface of an oil substrate. Shear separation will then be applied to prevent complete gelation, promoting particle-particle interactions. Therefore the production of emulsion fluid gels has been investigated, with particular attention to the resulting rheological properties.

2. Materials and Methods

2.1. Materials

Whey protein isolate (WPI) was obtained from Kerry Ingredients, Listowel, Ireland (WPI, W994, S-493391) and used without further purification. WPI composition as stated by the supplier was 91.0% protein, moisture 4.0%, fat 1.0%, ash 3.5% and lactose 0.5%. Mineral content of the WPI was: Ca – 0.50, P – 0.65, Na – 0.10, K – 0.15, Mg – 0.02 and Cl - 0.02%. High oleic sunflower oil was obtained from Cargill (Cargill Inc., BE). Sodium azide, hydrochloric acid, silicon oil, Nile Red and Rhodamine B were purchased from Sigma-Aldrich (Sigma-Aldrich, UK).

2.2. Preparation of oil filled fluid gels

Preparation of the oil filled fluid gels involved a three-step process. Primary solutions of WPI were firstly prepared and used to form O/W emulsions. The emulsions were then heat treated under shear conditions resulting in emulsion fluid gels (EmFG).

125

126 *2.2.1. Preparation of WPI stock solutions*

127 Whey protein stock solutions (5 to 30 **wt**% on a protein basis) were
128 prepared by dispersing WPI in deionised water. An anti-microbial, sodium azide
129 (0.02 **wt**%) was added to all solutions to enhance storage times. Solutions were
130 stirred overnight at ambient conditions until completely hydrated and stored at
131 5 °C until further usage. For the preparation of stained samples Rhodamine B
132 (0.015 mM) was added to stain the protein. Stained samples were kept covered
133 to prevent photo bleaching.

134

135 *2.2.2. Preparation of emulsions*

136 Oil in water emulsions were prepared by the addition of high oleic oil to
137 WPI primary solution (Protein concentration ranging from 5 to 30 **wt**%) so that
138 total volumes resulted in oil fractions ranging from 5 to 20 **vol**%. The mixtures
139 were subsequently mixed in a high shear mixer (Silverson, SL2T) at 4000 rpm
140 for 10 minutes. System pH was adjusted to pH 4.6 with concentrated
141 hydrochloric acid (12 M) and aged for 72 hours before gelling under shear.
142 Stained EmFG were prepared with the addition of Nile Red (0.015 mM) to the oil
143 phase and kept covered to prevent photo bleaching.

144

145 *2.2.3. Preparation of oil filled fluid gels*

146 A jacketed vessel and overhead stirrer equipped with pitched blade
147 impeller was used to prepare all WPI emulsion fluid gels (EmFG). Aliquots of
148 emulsion were added to a jacketed vessel set to 50 °C, controlled through a
149 circulating water bath. Shear was applied through the stirrer and impeller at 450

rpm. Once thermal equilibrium was obtained (Ca. 10 minutes), emulsions were heated at a rate of 0.5 °Cmin^{-1} to 80 °C. Suspensions were subsequently decanted and left to cool quiescently under ambient conditions. Cooled EmFG were further stored at 5 °C for seven days until rheologically tested. In all experiments a cover was applied to minimise water loss. When staining, the system was covered in aluminium foil to avoid fluorescence quenching.

2.3. Static light scattering (SLS)

A MS2000 Mastersizer with attached Hydro SM manual small volume dispersion unit (Malvern Instruments Ltd, UK) was used to obtain size distributions for EmFG particles. Distributions are the average of three repeats. Particle size calculations were based upon the Mie theory, thus particles were assumed to be monodisperse, homogenous spheres. Additionally, once coated, particles were a binary system of protein and oil; as such the refractive index of the shell was used.

2.4. Microscopy

2.4.1. Optical light microscopy

Samples were prepared by first diluting the EmFG in deionised water (7.5 **vol**%). A Brunel SP300-fl (Brunel Microscopes Ltd, UK) optical light microscope fitted with an SLR camera (Cannon EOS Rebel XS, DS126 191) at 20 and 40x optical magnification was used to image the particles. Slides were prepared by addition of 50 μL of sample to a microscope slide (VWR, UK) and covered with a coverslip (Thickness no.1, VWR, UK).

175 *2.4.2. Confocal Laser scanning microscopy (CLSM)*

176 Stained samples prepared with both Rhodamine B and Nile Red were
177 imaged using concave microscope slides (60 μL), with a coverslip sealed using
178 super glue. Fluorescence free, UV transparent immersion oil (Sigma-Aldrich, UK)
179 was used to bridge the gap between coverslip and objective lens (40x
180 magnification). A Leica TCS-SPE confocal microscope (Leica Microsystems Ltd,
181 UK) fitted with an argon laser was used for all CLSM analysis. Rhodamine B
182 stained protein was excited at 532 nm and detected at 560-600 nm, and Nile Red
183 was excited at 488 nm and detected at 680-700 nm respectfully. 3-dimensional
184 images were obtained using 0.5 μm slices throughout. Further image processing
185 was undertaken using an image software package (ImageJ).

186

187 ***2.5. Rheological Analysis***

188 Rheometry was conducted using a Bohlin Gemini HR Nano stress-
189 controlled Rheometer (Malvern Instruments Ltd, UK) equipped with serrated
190 parallel plate (25 mm diameter) at 1 mm gap height. Experiments were
191 undertaken at 25 °C using a silicon oil moisture trap. An equilibrium was
192 achieved for 15 minutes prior to testing, allowing for consistent loading
193 conditions. Particle phase volumes were obtained using a method outlined by
194 Moakes, et al. [23]; whereby aliquots of a given volume were centrifuged, water
195 phase separated and volumes obtained. Phase volumes were calculated as
196 followed (equation 1):

197 $$Particle\ Phase\ Volume = 1 - \left(\frac{Volume\ of\ Water\ Removed}{Total\ Initial\ Volume}\right) \quad \text{Eq. [1]}$$

198

2.5.1. Yield stress determination

Yield stresses were determined as the stress at which the transition from storage modulus (G') to loss modulus (G'') dominance occurred; the G'/G'' cross over point on a stress controlled amplitude sweep. Amplitude sweeps were conducted at 1 Hz from 0.1 to 400 Pa.

2.5.2. Dynamic oscillatory measurements

Frequency sweeps were obtained between 0.1 and 10 Hz at controlled stress. The stress was determined by amplitude sweeps as a value within the linear viscoelastic region (LVR) for all EmFG tested. For samples containing no oil a, couette, double gap geometry was used: as the large surface area allowed lower values of G' to be probed in the lower viscosity fluids.

2.5.3. Viscosity measurements

Dynamic viscosity measurements were undertaken between 0.1 and 400 s^{-1}. Shear sweep time was set to 10 minutes (ramp ascending and descending). Two consecutive sweeps were run with the second commencing immediately after the first having been completed.

2.5.4. Recovery analysis

EmFG recovery was probed by primarily rejuvenating the system. A pre-shear (10 s^{-1} for 10 s) was applied to the system and subsequent change in storage modulus (G') recorded over the following 30 min. G' was obtained at 1Hz and 1 Pa.

2.6. Encapsulation efficiency

Optical microscopy was used to analyse oil droplet entrapment for each system. Micrographs of the raw emulsion were obtained and emulsion droplets in each image manually counted to give an average droplet count (N_{em}) determined over 12 images. Values for uncoated emulsion droplets (N_{fo}) in the final EmFG systems were then obtained in the same manner. An example of both a coated and uncoated droplet has been shown in figure 1. The ratio of the two was used to calculate the percentage of encapsulated oil, as shown in equation 2:

$$\%_{Encapsulated} = \left(1 - \frac{N_{fo}}{N_{em}}\right) \times 100 \qquad \text{Eq. [2]}$$

Encapsulation was averaged over 12 micrographs with error calculated as the 95% confidence interval.

3. Results and Discussion

3.1. Preparation of emulsion fluid gels (EmFG)

An O/W system where the excess WPI emulsifier exceeded the critical gelling concentration[28] (> 1 **wt**%), was subjected to heat treatment under shear conditions. The shear flow exerted on the system during the sol-gel transition prevented the formation of a continuous gel network, resulting in single discreet particles/encapsulates.

3.1.1. Encapsulation efficiency

Figure 2 shows the encapsulation efficiencies for systems with both increasing WPI concentration (a) and oil phase volume, ϕ_{oil}, (b). It was observed that high levels of encapsulation, ~99%, were achieved in systems with lower

WPI concentrations, however as the WPI exceeded 20 **wt**%, entrapment decreased. It is argued that the degree of encapsulation is closely correlated to the flow behaviour of the system during the sol-gel transition. It has previously been reported that around the isoelectric point of WPI (ca. pH 5) a transition from Newtonian to pseudoplastic flow occurs in systems containing 20 **wt**% whey protein, with yield stresses observed on further concentrated solutions[29, 30]. Such changes in the system viscosity retard or prevent the diffusion of denatured protein to the oil/water interface due to a reduction in mobility and increased collisions with other denatured polymer chains. In turn, both increased formation of WPI aggregates without included oil and free emulsion droplets were observed in the final suspensions.

Increasing the phase volume of the oil from 5 to 20% whilst retaining a standard WPI concentration (15 **wt**%) however, had little effect on the emulsion entrapment, yielding droplet entrapment in excess of 95%. Here, the increase in oil was not sufficient to raise the viscosity of the system, and hinder polymer diffusion. However, at low oil fractions increasing the WPI concentration from 5 to 15 **wt**% caused an observed transition from suspension creaming to sedimentation, indicating a change in particle density, probably as a result of a change in shell thickness.

3.1.2. Particle morphology

Particle morphology was studied using confocal laser scanning microscopy (CLSM). Previous reports regarding the formation of WPI microgel particles through the application of shear[23], show irregular shaped particles, characterised by a larger length to width ratio. However, the incorporation of oil

in to the system resulted in particles with spherical morphology, whereby a gel layer surrounded an oil substrate, as shown in figure 3.

Imaging the EmFG particles at 0.5 μm intervals gave enhanced topographical detail (figure 3a), allowing the coating to be observed. A non-uniform shell with much greater thickness than expected for emulsified droplets was shown, inferring the presence of a gel layer. Additionally, cross-sections were obtained using CLSM, which again show shell thickness and non-uniformity, but also through negative staining and dying, oil reservoirs in the centre of the particles (figures 3b and 3c respectfully).

The mechanism for particle formation is thought to be based upon the oil acting as a substrate for shell growth. Growth occurs through enrichment from the surrounding un-gelled biopolymer. Primarily led by the β-lactoglobumin, heat induced denaturation of the native structure causes hydrophobic regions to become exposed[31, 32]. Hydrophobic interactions then dominate the gelation causing diffusion of the denatured polymer to the oil/water interface. The oil droplet thus acts as a point for nucleation and growth. Shear imposed upon the system then restricts particle-particle aggregation, preventing a continuous network from forming. As a result, particles grow to an extent permitted by the shear flow, however are primarily dictated by the size of the emulsion droplets.

3.1.3. EmFG particle size distributions

Particle size distributions for all EmFG systems are shown in figure 4. It is clear from figure 4a that increasing WPI concentration results in a shift towards smaller particle sizes. Particles are primarily a function of the emulsion droplet size, thus such observations would be expected as increasing the emulsifier

298 concentration causes the formation of smaller droplets[33, 34]. However, by further
299 increasing the protein concentration up to 30 **wt**%, the formation of a bimodal
300 system centred at ~9 μm, with a second peak at much higher particle sizes
301 (~200 μm) was observed. The shift from monomodal to bimodal is due to the
302 formation of gelled particles where no oil has been entrapped as observed
303 through microscopy. As previously described, the change in system flow results
304 in aggregated protein, as diffusion of the denatured polymer becomes restricted,
305 causing a transition from protein-substrate to protein-protein interactions. The
306 extent of such a transition is thus reflected by the change in peak intensity
307 observed in systems with 20 to 30 **wt**% WPI.

308 Figure 4b shows little effect on the resulting particle size as a function of
309 oil fraction, as a result of consistent emulsifier concentrations and unrestricted
310 diffusion of biopolymer to the substrate interface. Thus, all distributions are
311 centred around 25-30 μm complimenting sizes observed via microscopy (figures
312 1 and 3).

313

314 ***3.2. EmFG material properties***

315 *3.2.1. Small deformation oscillation testing*

316 To further understand and characterise the EmFG physico-mechanical
317 properties, small deformation rheology was carried out. Figure 5a shows
318 frequency sweeps obtained for EmFG systems prepared with varying oil
319 fractions from 0 to 20 **vol**%. Systems containing no oil displayed typical liquid-
320 like behaviour where both moduli were dependent on frequency and G'' is higher
321 than G' throughout the measured frequency range[35]. The addition of oil caused a
322 transition in rheological behaviour to pseudo-solid where G' is higher than G'',

with both moduli becoming further independent to frequency as a function of the oil. Here particle proximity is such that inter-particle interactions arise as observed for WPI microgel particles[23], however, as the shear and thermal history exerted was consistent across all systems, it is argued that system elasticity becomes a function of the oil content; where increasing oil fractions increase the effective phase volumes of the particles, as shown in figure 5b.

To better understand the mechanism through which system elasticity arises, the results obtained have been compared to models already proposed for particulate suspensions. The Krieger-Dougherty (KD) model is used to describe the relationship between relative viscosity (η_{rel}) and particle phase volume for hard sphere suspensions[36], equation 2.

$$\eta_{rel} = \left(1 - \frac{\phi}{\phi_{max}}\right)^{-[\eta]\phi_{max}} \quad \text{Eq. [2]}$$

The equation relates the ratio between the phase volume of the suspension, ϕ, to the maximum packing fraction for monodisperse hard spheres (0.64), ϕ_{max}, as a function of the intrinsic viscosity, $[\eta]$. What is clear from equation 2 is that as the maximum packing fraction is approached the relative viscosity will asymptote and eventually the equation fail as the suspension reaches/surpasses the maximum packing. As such, the KD equation cannot be used to describe the correlation observed in figure 5b, where the maximum packing fraction for hard spheres has been exceeded.

Similar observations have been reported for agar microgel suspensions[9], where above a critical volume fraction, ϕ_c, elastic response was observed, becoming insensitive to phase volumes above ϕ_{max}. It was explained that above ϕ_c, elasticity was a function of the particle modulus; hence particles were

typically acting as soft spheres, however the plateauing effect was left unexplained, suggested as an artefact of the phase volume calculation. EmFG are therefore assumed to act as soft spheres. It is suggested that the soft oil core and elastic whey protein shell allows for particle deformation when highly concentrated, reaching phase volumes that exceed those expected for rigid spheres. At such high phase volumes a jamming phenomenon is observed, thus particle rheology mainly represents a function of the shell[37]. Hence above a volume fraction of 0.64 particles are packed to an extent that system elasticity is close to those shown for filled quiescent gels[38], hence frequency sweeps show gel-like behaviour (figure 5a).

EmFG prepared using 5 **vol**% oil showed marked storage moduli even though ϕ_{max} had not been reached. Here, elastic response is observed not through the jamming of particles, but assumed to arise from particle trapping as a result of steric confinement through inter-particle interactions. Between ϕ_c and ϕ_{max} it is argued that EmFG act as a glass where particles become trapped allowing localised motion but not long range diffusion, similarly to results published by Koumakis, et al. [37] and Le Grand [39]. Therefore, the EmFG can be categorised into three regimes; suspended particles below ϕ_c, glassy between ϕ_c and ϕ_{max}, and jammed above ϕ_{max}.

3.2.2. Material yielding behaviour

The effect of oil fraction on material response was further probed through the use of stress sweeps. Figure 6 shows the data obtained for EmFG with increasing oil content (from (a) to (d)). The stress sweeps indicate that at a critical stress the network started to break down. Further increasing the stress

led to a transition at which point the loss modulus dominated the storage. At this point a change in material response occurs, where the system no longer resembles a pseudo-solid, but is much more fluid-like. For systems in a glassy state, where particle have become trapped through inter-particle interactions, the linear viscoelastic region (LVR) was observed to be much shorter than those that are jammed. Again, such observations can be interpreted through the deformability of the particles; where particles are in close proximity they become compressed and deform, a larger stress is needed to induce flow as observed for κ-carrageenan fluid gels[6]. However, for systems where ϕ does not surpass ϕ_{max}, particles appear to act as hard spheres, as such deformation does not occur which is reflected by the lower stresses required to induce flow[39], as shown in figure 7. Here it is possible to see a similar correlation as observed for the frequency sweeps, where a plateau is reached for oil fractions above 10 **vol**%. This yielding insensitivity towards increasing oil fractions again infers a network of deformed particles closely packed together, as previously suggested[39].

3.2.3. Suspension flow behaviour

System flow behaviours for all WPI EmFG were studied and presented in figure 8. EmFG showed marked shear thinning behaviours typical of highly flocculated suspensions[40]. At very low shear rates (~0.01 s^{-1}) an apparent shear thickening can be observed as a resultant effect of soft jamming. Continued increase in the applied strain resulted in thinning of the suspensions. The observed thinning is due to the inhomogeneous flow across the shear profile applied, as a result of the break down to the weakly flocculated network[40]. Thus

a degree of inter-particle interactions is suggested, where initially clusters of mesostructures are broken down to form single mesostructures (smaller flocs) and eventually microstructures (single particles). To analyse this further, data has been presented for the ramp up, down and additionally a second sweep taken immediately after the first.

The presence of hysteresis highlighted a thixotropic nature arising through the breakdown of floccules and inter-particle interactions, as seen in figure 9. The plot shows a similar correlation as previously observed for yield stresses and frequency sweeps whereby the highly packed systems (10 to 20 **vol**% oil) have a greater hysteresis. This indicates that jammed systems have a much higher degree of inter-particle interactions as a result of greater packing arising through particle deformation. As expected, where the particles remain unjammed a lower degree of thixotropy is observed, as non-deformed particles present a smaller surface area for inter-particle interactions to occur. However, data obtained for the second sweep showed a similar thixotropic behaviour for all systems, irrespective of oil content. Additionally, a combination of microscopy and light scattering techniques showed that the applied shear was insufficient to break the single particles, with the same particle size distributions observed pre and post shear sweeps (data not shown). As such it is argued that the shear applied throughout the first sweep disrupts the network to an extent that all particles behave as independent spheres. This is followed by restructuring between the particles, but on a scale that is much slower than the break down.

3.2.4. Material recovery

The recovery was further probed using oscillatory rheology. Primarily the system underwent rejuvenation, whereby the flocculated structure is broken down at a shear rate found within the shear-thinning region for all systems (10 s^{-1} for 10 s). The structuring was then observed through the storage modulus (G') over the subsequent 30 min, figure 10. The recovery curves show a two-step process, initially rapid, followed by a more gradual increase in elastic modulus, observed as a power function (0.45±0.7). The same power law dependency observed across all systems can be argued as the same recovery mechanism being observed *ie*. Initially there is rapid formation of a large number of small flocs, as the flocs grow in size the change in G' slows as fewer larger particles are available to interact. The extent and rate of recovery however was dependent on the volume fraction of the particles. Volume fractions greater than 0.64 could not be significantly differentiated, with the extent and rate of recovery depending on the self-similarity of the shells. For EmFG <0.64, G' values were lower by a factor of 10; as is observed from the frequency sweep data, again due to much less interacting where particles are further apart in space. As such, the hysteresis observed through dynamic shear experiments is suggested to arise not through the rupturing of a weakly gelled structure, but from the break down of reversible interactions between the particles.

4. Conclusions

This study has shown that oil droplets can be incorporated into a WPI gel layer by applying a shear-gel technique. Entrapment efficiency was observed to be dependant on the protein concentration, as a function of the viscosity and flow behaviours, reaching up to 99% encapsulation. By applying shear during the

WPI sol-gel transition discreet micron sized spherical capsules were obtained, with enhanced structuring properties. Small deformation rheology was used to characterise the suspensions, which showed pseudo-solid like behaviour at rest, however, by applying a shear force to the system that is greater than the yield stress, the suspensions could be made to flow. Suspension rheology highlighted a significant dependence on the oil fraction, with the addition of oil increasing the effective phase volume of the particles, resulting in an increase in particle proximity. Increasing the oil content to around 10 **vol**% led to packing fractions that exceeded those for hard spheres. As such, particle properties have been expressed as soft and deformable. Flow behaviours of the suspensions were indicative of highly flocculated systems, where marked shear thinning was observed through the break up of weakly aggregated flocs and mesostructures. Furthermore, when left under quiescent conditions the particulate suspensions showed significant recovery, displaying the occurrence of reversible interactions.

Acknowledgements

The authors would like to thank the sponsoring bodies including EPSRC, Kerry Group, and also Birmingham Science City: Innovative Uses for Advanced Materials in the Modern World (West Midlands Centre for Advanced Materials Project 2), with support from Advantage West Midlands (AWM) and part funded by the European Regional Development Fun (ERDF), for the use of the confocal microscope used in this research.

References

1. I. T. Norton, D. A. Jarvis and T. J. Foster, *International journal of biological macromolecules*, 1999, **26**, 255-261.
2. N. Altmann, J. J. Cooper-White, D. E. Dunstan and J. R. Stokes, *Journal of Non-Newtonian Fluid Mechanics*, 2004, **124**, 129-136.
3. J. E. Norton and I. T. Norton, *Soft Matter*, 2010, **6**, 3735-3742.
4. I. Fernández Farrés, R. J. A. Moakes and I. T. Norton, *Food Hydrocolloids*, 2014, **42, Part 3**, 362-372.
5. C. L. A. Berli and D. Quemada, *Langmuir : the ACS journal of surfaces and colloids*, 2000, **16**, 7968-7974.
6. D. A. Garrec, B. Guthrie and I. T. Norton, *Food Hydrocolloids*, 2013, **33**, 151-159.
7. I. Fernández Farrés, M. Douaire and I. T. Norton, *Food Hydrocolloids*, 2013, **32**, 115-122.
8. A. Gabriele, F. Spyropoulos and I. T. Norton, *Food Hydrocolloids*, 2009, **23**, 2054-2061.
9. S. Adams, W. J. Frith and J. R. Stokes, *Journal of Rheology*, 2004, **48**, 1195.
10. E. Çakır and E. A. Foegeding, *Food Hydrocolloids*, 2011, **25**, 1538-1546.
11. S. M. Fitzsimons, D. M. Mulvihill and E. R. Morris, *Food Hydrocolloids*, 2008, **22**, 485-491.
12. K. Nishinari, H. Zhang and S. Ikeda, *Current Opinion in Colloid and Interface Science*, 2000, **5**, 195-201.
13. I. T. Norton and W. J. Frith, *Food Hydrocolloids*, 2001, **15**, 543-553.
14. C. Rocha, J. A. Teixeira, L. Hilliou, P. Sampaio and M. P. Gonçalves, *Food Hydrocolloids*, 2009, **23**, 1734-1745.
15. T. Van Vliet, *Colloid and Polymer Science*, 1988, **266**, 518-524.
16. D. B. Genovese, *Advanced Colloid and Interface Science*, 2012, **171-172**, 1-16.
17. E. Dickinson and J. Chen, *Journal of Dispersion Science and Technology*, 1999, **20**, 197-213.
18. E. Dickinson, *Journal of the Chemical Society, Faraday Transactions*, 1998, **94**, 1657-1669.
19. E. Dickinson and Y. Matsumura, *International journal of biological macromolecules*, 1991, **13**, 26-30.
20. D. Sağlam, P. Venema, R. de Vries, L. M. C. Sagis and E. Van Der Linden, *Food Hydrocolloids*, 2011, **25**, 1139-1148.
21. A. Sullo, R. L. Watson and I. T. Norton, in *Gums and Stabilisers for the Food Industry 17: The Changing Face of Food Manufacture: The Role of Hydrocolloids*, The Royal Society of Chemistry, 2014, pp. 287-302.
22. D. A. Garrec and I. T. Norton, *Journal of Food Engineering*, 2012, **112**, 175-182.
23. R. J. A. Moakes, A. Sullo and I. T. Norton, *Food Hydrocolloids*, 2015, **45**, 227-235.
24. C. Chung, B. Degner, E. A. Decker and D. J. McClements, *Innovative Food Science & Emerging Technologies*, 2013, **20**, 324-334.
25. A. Matalanis and D. J. McClements, *Food Hydrocolloids*, 2013, **31**, 15-25.
26. Z. Zhang, R. Zhang, E. A. Decker and D. J. McClements, *Food Hydrocolloids*, 2015, **44**, 345-352.
27. A. I. Romoscanu and R. Mezzenga, *Langmuir : the ACS journal of surfaces and colloids*, 2006, **22**, 7812-7818.

28. M. Stading and A.-M. Hermansson, *Food Hydrocolloids*, 1990, **4**, 121-135.
29. P. Walkenstrom, E. Windhab and A.-M. Hermansson, *Food Hydrocolloids*, 1998, **12**, 459-468.
30. A. M. Hermansson, *Journal of Texture Studies*, 1975, **5**, 425-439.
31. M. A. M. Hoffmann, S. P. F. M. Roefs, M. Verheul, P. J. J. M. Van Mil and C. G. De Kruif, *Journal of Dairy Research*, 1996, **63**, 423-440.
32. W. H. Sawyer, *Journal of dairy science*, 1968, **51**, 323-329.
33. D. J. McClements, *Food Emulsions Principles, Practices, and Techniques*, CRC Press, 2005.
34. P. Walstra, *Chemical Engineering Science*, 1993, **48**, 333-349.
35. S. B. Ross-Murphy, *Polymer Gels and Networks*, 1994, **2**, 229-237.
36. I. M. Krieger and T. J. Dougherty, *Journal of Rheology*, 1959, **3**, 137-152.
37. N. Koumakis, A. Pamvouxoglou, A. S. Poulos and G. Petekidis, *Soft Matter*, 2012, **8**, 4271-4284.
38. J. Chen, E. Dickinson, M. Langton and A.-M. Hermansson, *LWT - Food Science and Technology*, 2000, **33**, 299-307.
39. A. P. Le Grand, G., *Rheologica Acta*, 2008, **47**, 579-590.
40. D. Quemada, *The European Physical Journal of Applied Physics*, 1998, **1**, 119-127.

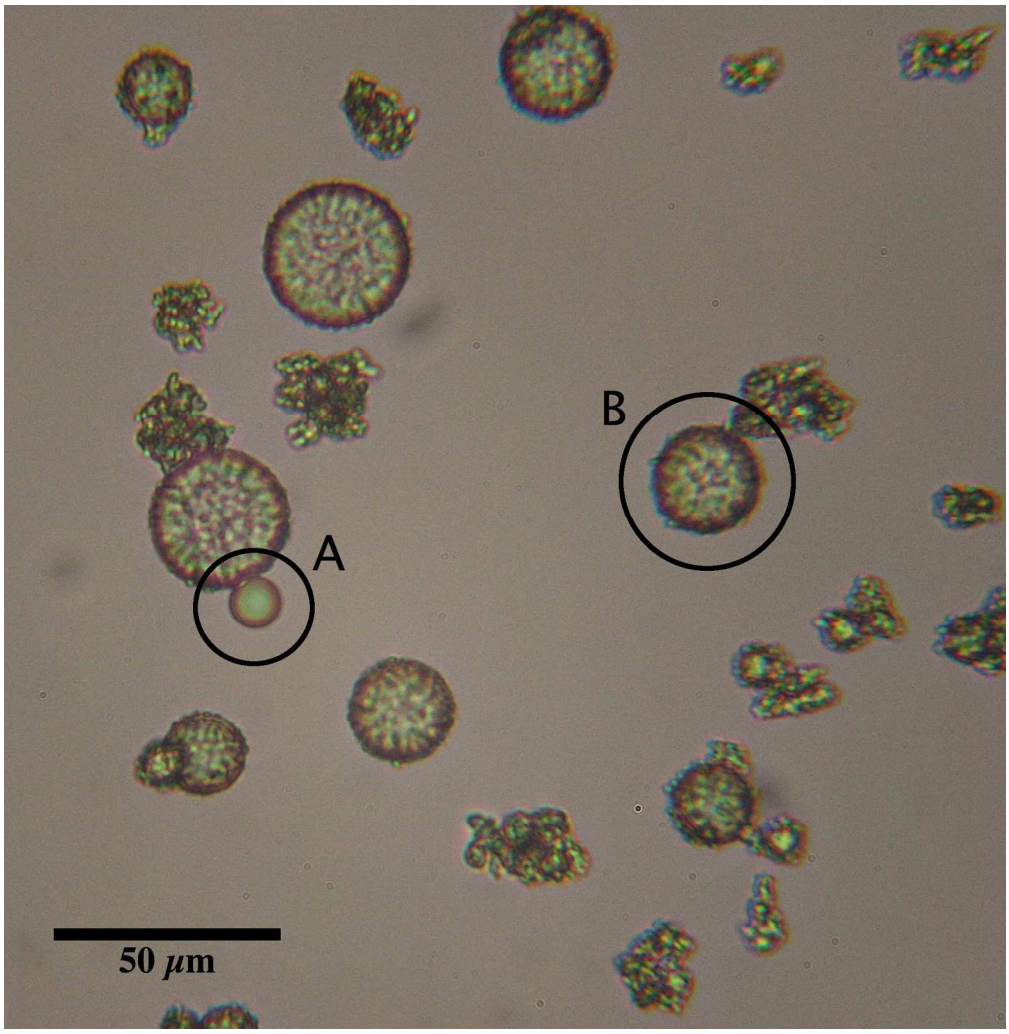

Figure 1: Optical micrograph highlighting (A) an uncoated oil droplet and (B) a coated EmFG particle.
738x753mm (72 x 72 DPI)

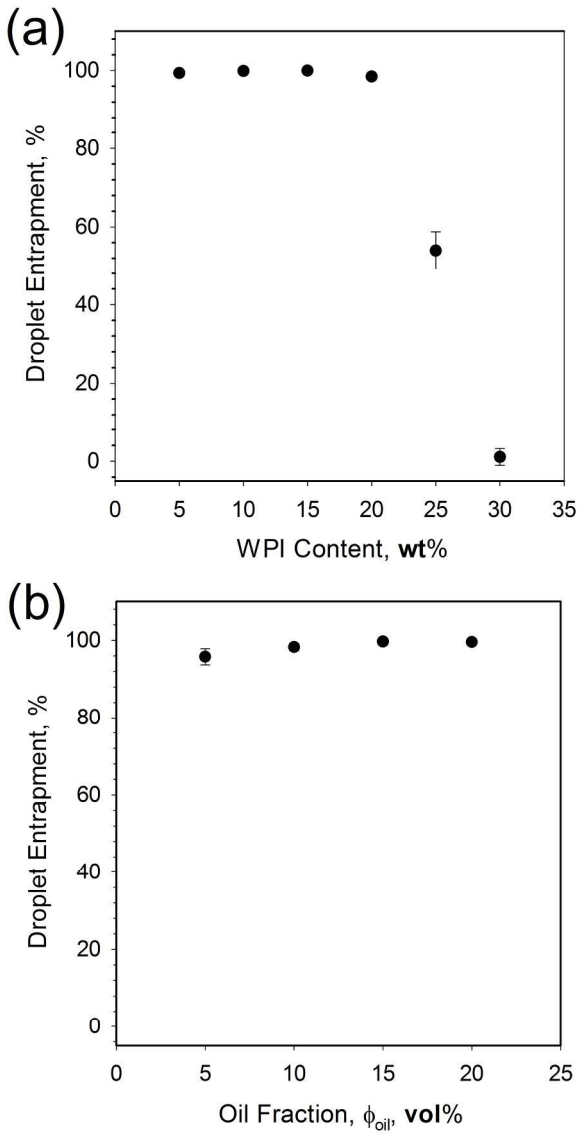

Figure 2: Oil droplet entrapment efficiencies for (a) EmFG systems prepared with increasing WPI concentrations ranging between 5 and 30 wt% at a fixed φoil of 10 vol%, and (b) EmFG systems prepared with increasing φoil between 5 and 20 vol% with a fixed WPI concentration of 15 wt%.
188x330mm (300 x 300 DPI)

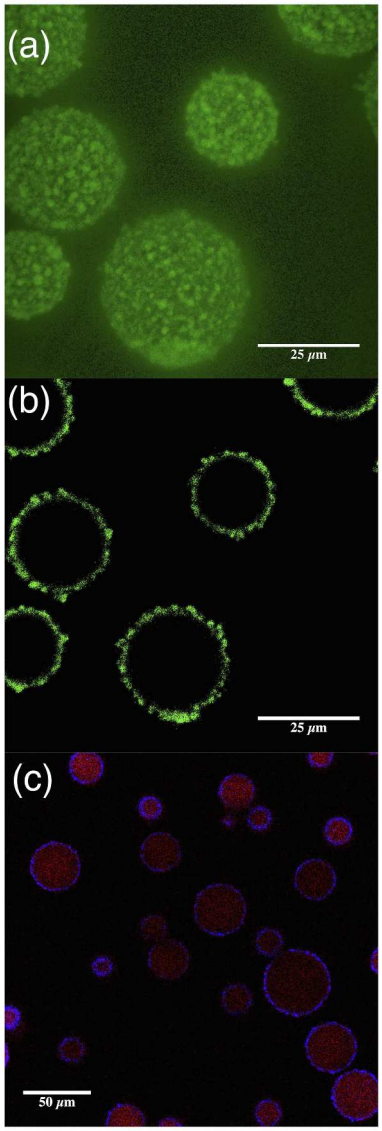

Figure 3: CLSM micrographs of EmFG particles. Gel phase has been stained using Rhodamine B (excitation wavelength: 532 nm, emission wavelength: 560-600 nm) and oil phase either negatively stained or stained using Nile red (excitation wavelength: 488 nm, emission wavelength: 690-700 nm). (a) 3D stack showing topographical detail of the EmFG particles, (b) cross section depicting stained gel layer surrounding a negatively stained oil core, and (c) stained cross section showing protein shell (blue) and oil core (red). Scale bars represent 25 μm (a and b) and 50 μm (c).
256x658mm (300 x 300 DPI)

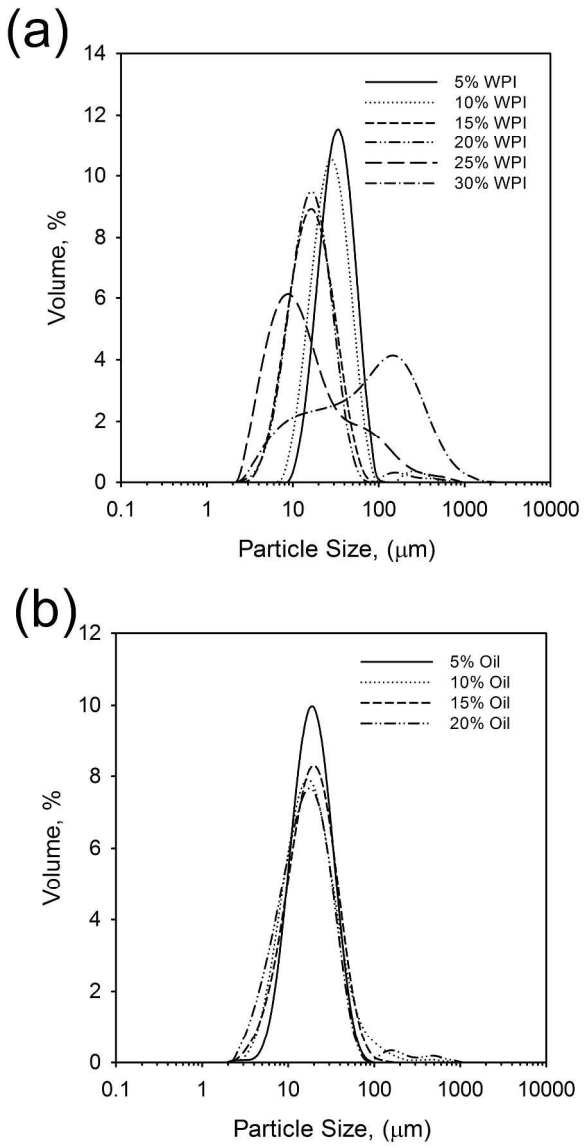

Figure 4: Particle size distributions for (a) EmFG prepared with a range of WPI concentrations between 5 and 30 wt% with a fixed φoil of 10 vol%, and (b) EmFG prepared with a range of φoil from 5 to 20 vol% with a fixed WPI content of 20 wt%.
228x425mm (300 x 300 DPI)

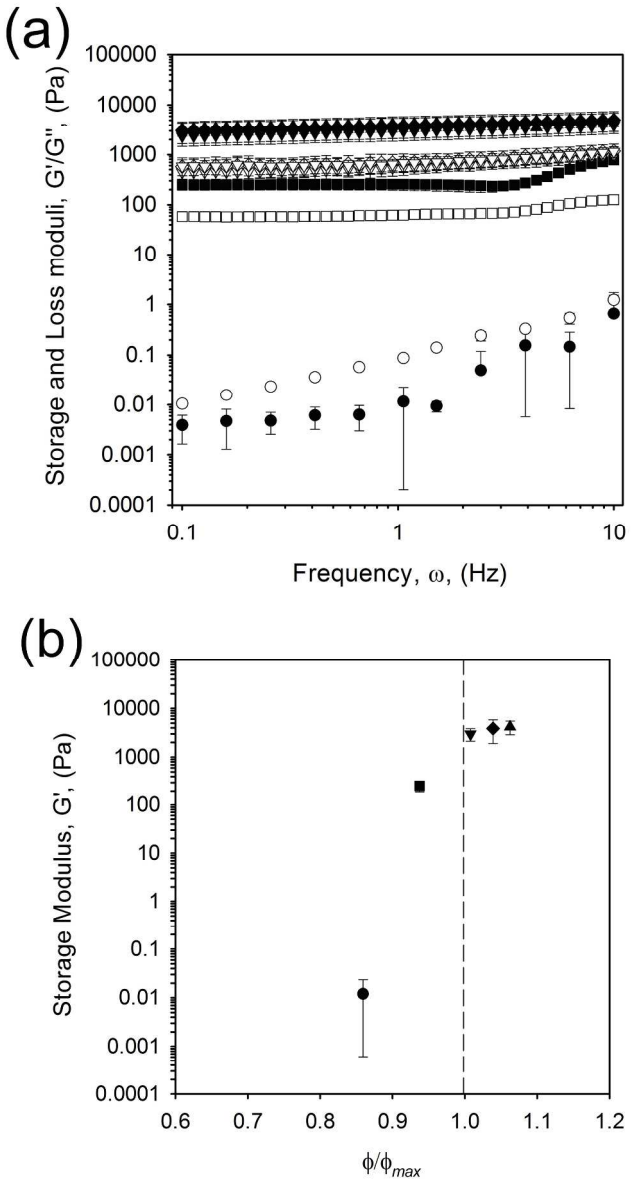

Figure 5: (a) Frequency sweeps obtained for EmFG prepared using 20 wt% WPI and (□,□) no oil, (′,≤) 5 vol% oil, (θ,σ) 10 vol% oil, (⌟,↓) 15 vol% oil, and (π,ρ) 20 vol% oil. Open markers represent the storage moduli (G′) and closed show loss moduli (G′′). (b) Storage modulus at 1 Hz verses particle phase volume for systems containing (□) no oil, (′) 5 vol% oil, (θ) 10 vol% oil, (⌟) 15 vol% oil, and (π) 20 vol% oil. Dashed line represents maximum packing faction for hard spheres.
214x352mm (300 x 300 DPI)

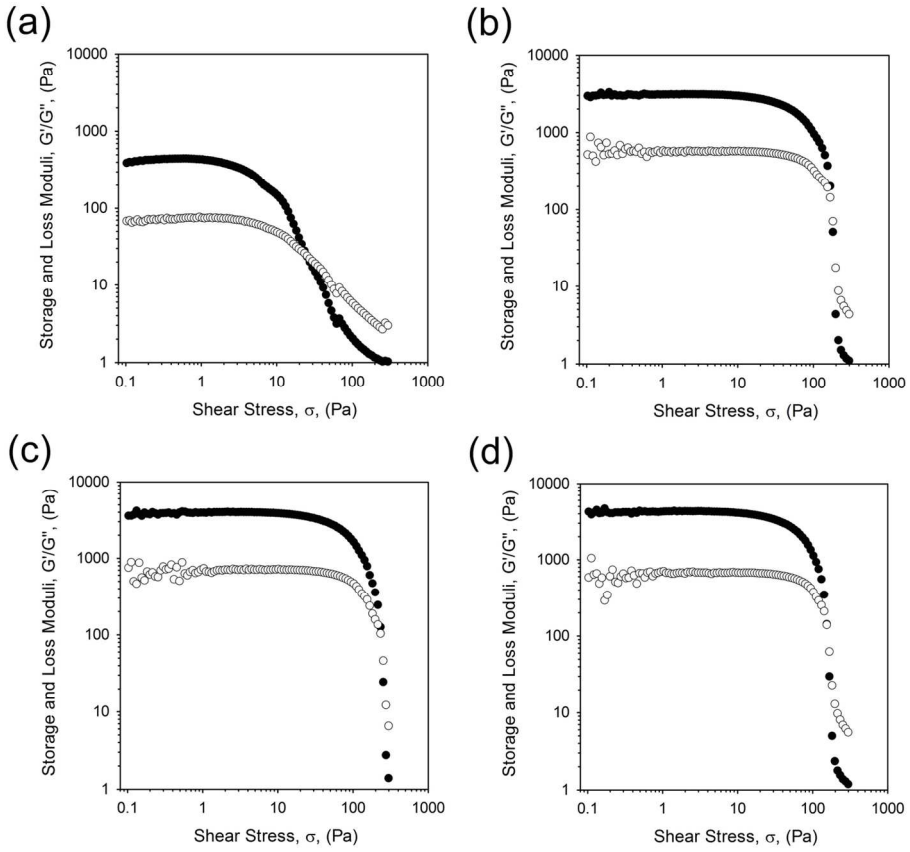

Figure 6: Stress sweeps obtained at 1 Hz for EmFG prepared with 20 wt% WPI and (a) 5 vol% oil, (b) 10 vol% oil, (c) 15 vol% oil, and (d) 20 vol% oil.
141x132mm (300 x 300 DPI)

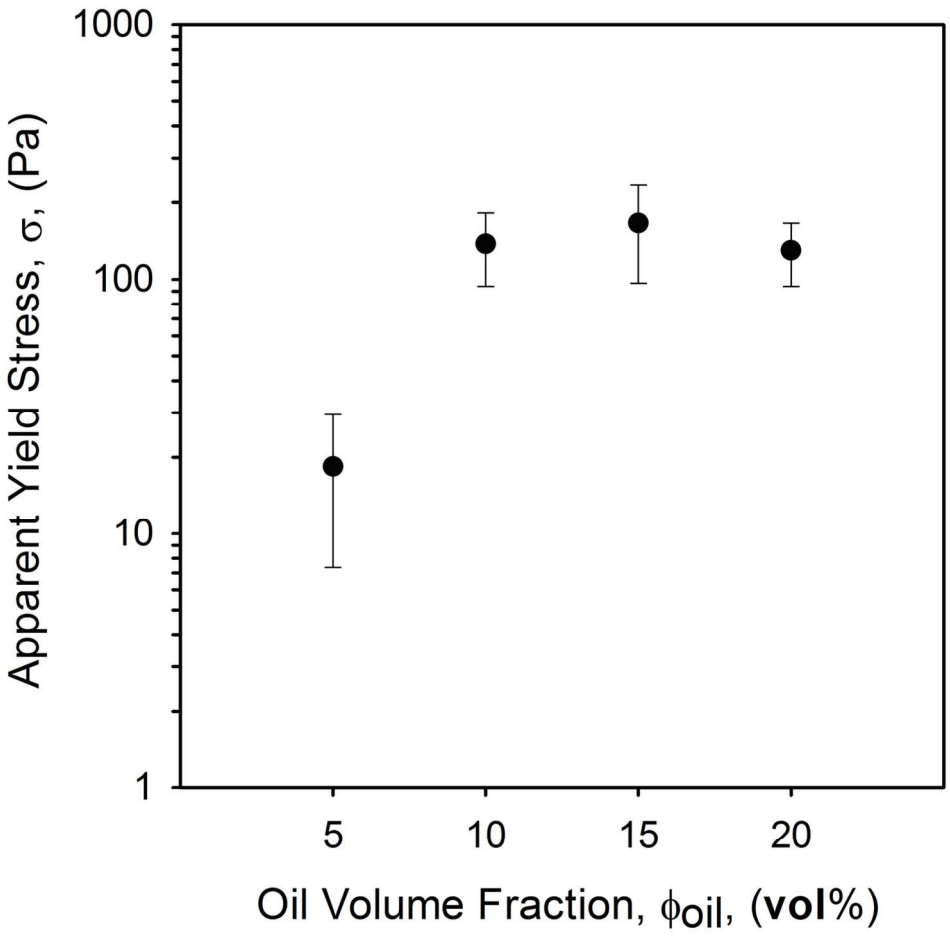

Figure 7: Apparent yield stresses determined using stress sweeps, as the point at which the storage modulus (G') cross the loss modulus (G'') for EmFG systems prepared using 20 wt% WPI and oil fractions between 5 and 20 vol%.
132x126mm (300 x 300 DPI)

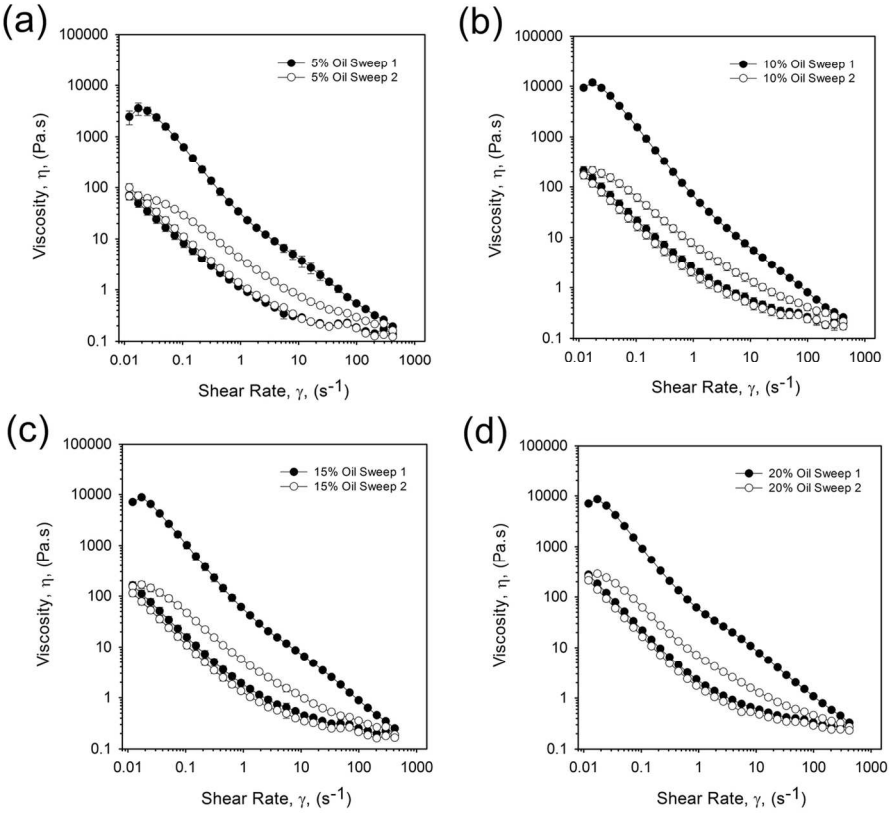

Figure 8: Viscosity profiles obtained for 20 wt% WPI EmFG containing (a) 5 vol% oil, (b) 10 vol% oil, (c) 15 vol% oil, and (d) 20 vol% oil. Closed markers represent sweep 1 and open, sweep 2.
137x123mm (300 x 300 DPI)

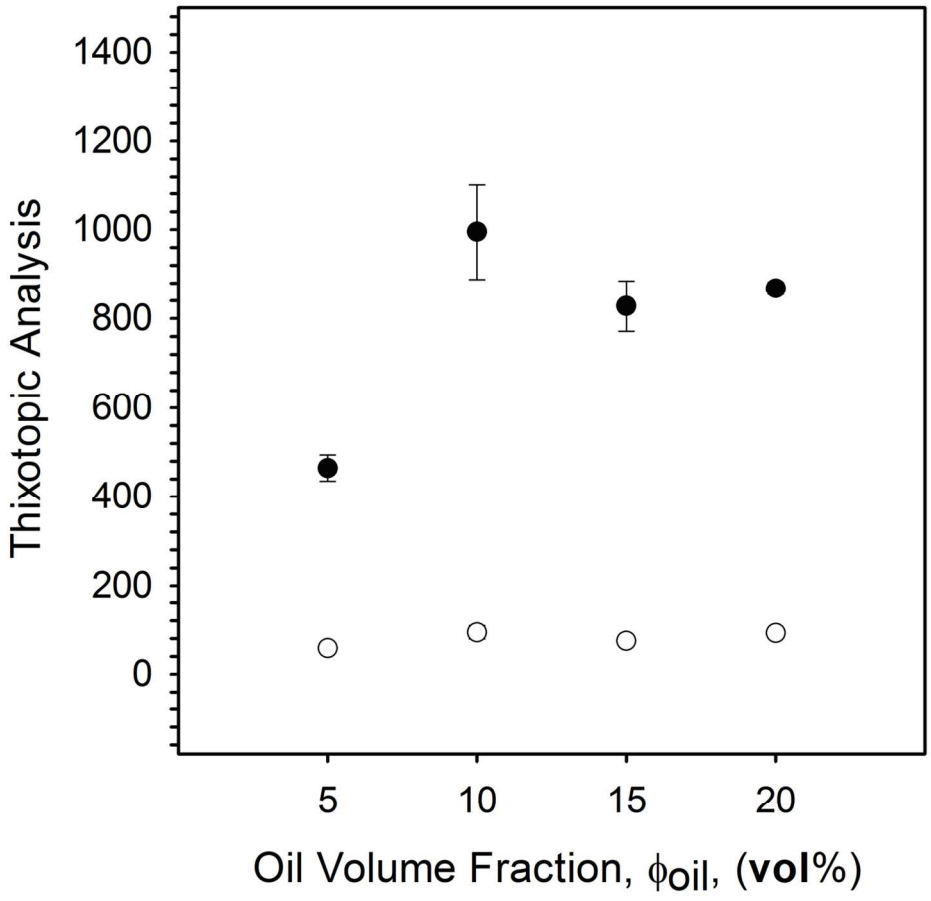

Figure 9: Thixotropic analysis obtained as the area between the viscosity profiles for 20 wt% WPI EmFG with increasing oil phase volumes from 5 to 20 vol% (□) denote thixotropic analysis for sweep 1 and (□) denotes values for sweep 2).
129x118mm (300 x 300 DPI)

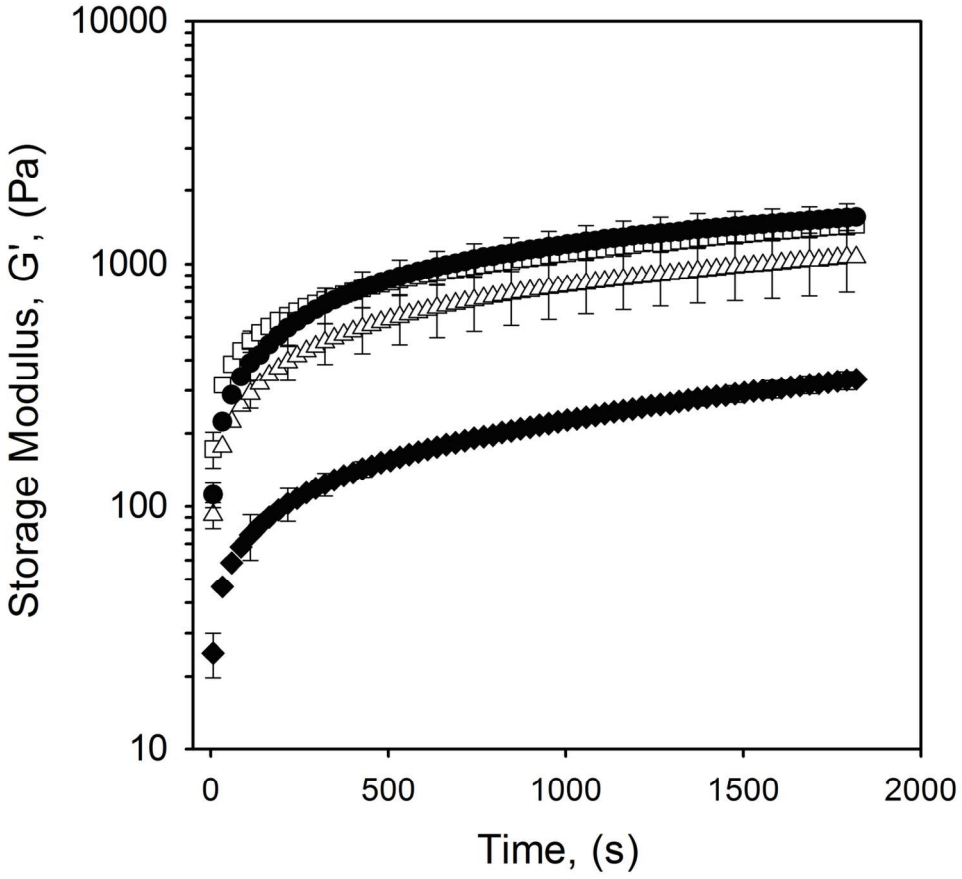

Figure 10: Storage modulus as a function of time for EmFG systems (↵) 5 vol% oil, (≤) 10 vol% oil, (ρ) 15 vol% oil, and (□) 20 vol% oil. All EmFG underwent a rejuvenation process of 10 s-1 for 10 s before measuring G' at 1 Hz and 1 Pa stress for 30 minutes.
127x114mm (300 x 300 DPI)

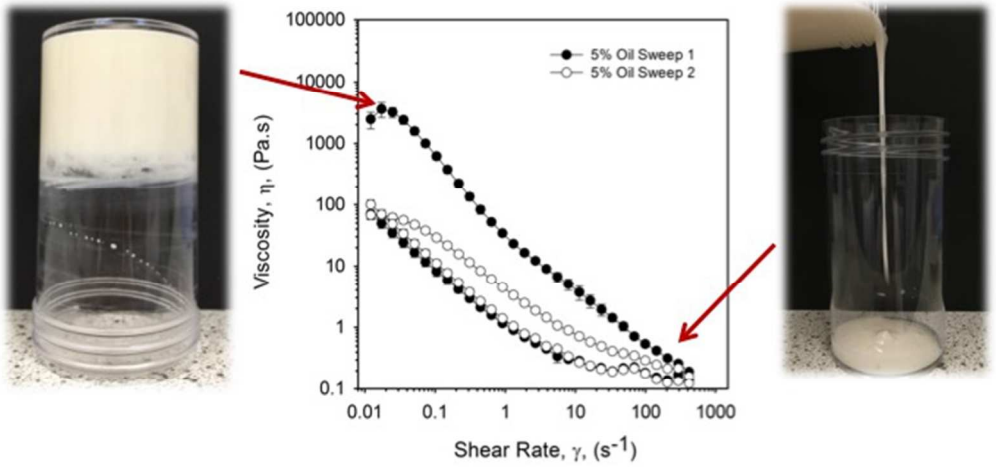

240x115mm (72 x 72 DPI)

The research uses a novel approach to tackle structuring in liquids through shear-gel technology, resulting in advanced material properties.